J. Mech. Phys. Solids 165 (2022) 104928

Contents lists available at ScienceDirect

Journal of the Mechanics and Physics of Solids

journal homepage: www.elsevier.com/locate/jmps

Membrane stretching based creep damage analytical solutions for thin disc small punch problem

Raheeg Ragab [a,*], Tao Liu [a,*], Ming Li [b,*], Wei Sun [c]

[a] Composites Research Group, Faculty of Engineering, University of Nottingham, University Park, Nottingham, NG7 2RD, United Kingdom
[b] School of Mechanics, Civil Engineering and Architecture, Northwestern Polytechnical University, Xi'an 710072, China
[c] Faculty of Engineering, University of Nottingham, University Park, Nottingham, NG7 2RD, United Kingdom

ARTICLE INFO

Keywords:
Small punch
Creep
Continuum damage mechanics
Membrane stretching

ABSTRACT

The small punch creep test (SPCT) presents a novel miniaturized testing technique popularly used to characterise creep and damage properties of high-temperature materials. Due to the complex non-linear deformation behaviour in the SPCT, a mechanistic based analytical solution describing creep deformation and damage in the SPCT remains unsolved so far. Instead, simplified empirical relations for the analysis of the SPCTs and data interpretation are often employed. However, such approaches lack theoretical underpinnings and thereby limiting the potential of the SPCT as a standardised material characterisation method. In this study, for the first time, creep damage analytical solutions were proposed to represent the complex deformation mechanism of the thin-disk small punch creep problem. The theoretical framework was established based on the membrane stretching theory and continuum damage mechanics-based constitutive model. The accuracy of the proposed analytical model was verified using finite element analysis. The analytical solutions demonstrated excellent capabilities and advantages over the existing models. Further, the potential applications of the new solutions were addressed. The proposed solutions represent a first key step towards improved theoretical modelling of the SPCT for ductile materials.

1. Introduction

Miniaturised creep test techniques, such as small punch test (Manahan, 1983; Parker and James, 1994), impression creep test (Hyde et al., 1996), and small ring test (Hyde and Sun, 2009; Sun and Hyde, 2010), have received an increasing attention over the last decade due to the small amounts of material required for sampling, thereby offering significant cost reductions and flexibility (Morris et al., 2018; Rouse et al., 2013). Amongst these tests, the small punch test has been increasingly applied to characterise creep properties (W. Wen et al., 2019; Al-Abedy et al., 2018; Kumar and Laha, 2015) and to acquire information on other mechanical properties such as tensile (Chen et al., 2020; Leclerc et al., 2021; Peng et al., 2021), fracture (Pham and Iwamoto, 2018) and fatigue (Lancaster et al., 2019) where only limited amounts of materials are available such as thin films, heat-affected zone of the weld (Gülçimen and Hähner, 2013), hazardous materials in the nuclear industry (Rabenberg et al., 2014), coating (G.A. Jackson et al., 2019; W. Wen et al., 2019) and additive manufactured materials (Torres and Gordon, 2021). The small punch creep test (SPCT), schematically shown in Fig. 1, typically involves the application of a constant load on a hemispherical punch to the surface of a circular thin flat disc specimen of

* Corresponding authors.
E-mail addresses: Raheeg.Ragab@nottingham.ac.uk (R. Ragab), Tao.Liu@nottingham.ac.uk (T. Liu), ming.li1@nwpu.edu.cn (M. Li).

https://doi.org/10.1016/j.jmps.2022.104928
Received 26 December 2021; Received in revised form 1 May 2022; Accepted 5 May 2022
Available online 7 May 2022

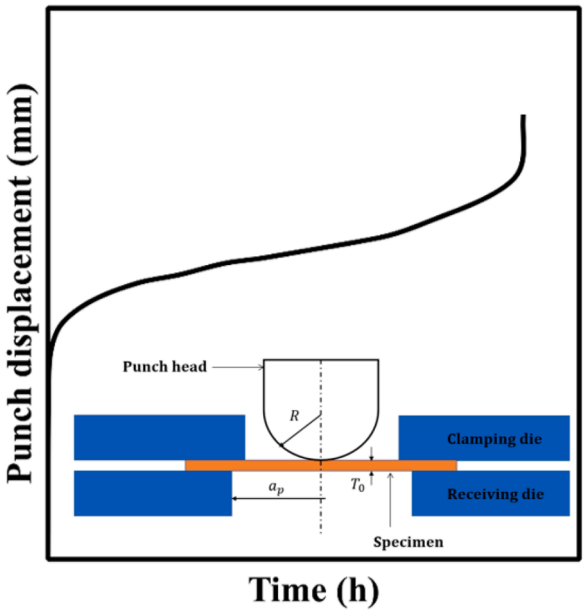

Fig. 1. A Schematic diagram showing the small punch creep test (SPCT) setup and a typical experimental SPCT curve with primary, secondary and tertiary creep stages.

3–10 mm in diameter and 0.2–0.5 mm in thickness (Rouse et al., 2013) to produce the small punch creep curve schematically illustrated by Fig. 1. Compared with other small-scale creep testing methods, the SPCT offers a key advantage in that it can characterise the full creep stages, i.e., primary, secondary and tertiary creep (Morris et al., 2018; Hyde et al., 2013), as shown schematically in Fig. 1. At elevated temperatures, determination of tertiary creep behaviour and creep damage properties become an essential requirement to maintain structural integrity of components and to estimate the remaining life.

Over the last 20 years, numerous experimental and numerical studies have been conducted to understand mechanics behaviour and physical mechanisms and to develop effective method to apply the small punch test for material characterisation (e.g., refs (Calaf-Chica et al., 2021; Dymáček et al., 2019; L. Zhao et al., 2019; Song et al., 2019; Ortiz-Mariscal et al., 2018; Yang et al., 2018; Cortellino et al., 2017; Cacciapuoti et al., 2016; Cortellino et al., 2016; Ma et al., 2009; G.A. Jackson et al., 2019)), reflecting a growing interest in this area and the progress made by the research community. However, interpretation of the experimental data obtained from small punch tests still remains a key challenge due to the complex interaction of various mechanisms such as material non-linearity, large deformations and strains, non-linear contact and initial plasticity effects (Rouse et al., 2013; Cacciapuoti et al., 2016). Some attempts have been made towards improving SPCT modelling and data interpretation through analytical methods, empirical based approaches and inverse finite element methods (W. Wen et al., 2019; Hyde et al., 2013; CEN 2006; T.H Hyde et al., 2010; Hyde et al., 2007; Dyson et al., 2016; Lee et al., 2016). The Chakrabarty theory for membrane stretching of circular blanks over a rigid hemispherical punch (Chakrabarty, 1970) offers a comprehensive analytical description of the local stresses and strains in a thin disc of isotropic material under membrane deformation mode, and therefore, it has been widely utilized for SPCT data interpretation and correlation since large deformations are considered and the geometry and loading conditions are similar to those in SPCTs (Rouse et al., 2013). Based on Chakrabarty model, the CEN code of practice (CEN 2006) proposed a methodology to correlate the experimental outputs of small punch creep tests to those obtained by conventional uniaxial creep tests. However, one of the main limitations of Chakrabarty theory when applied to small punch creep problems manifests in that it is strictly valid for a rigid plastic material behaviour model (Chakrabarty, 1970) and therefore creep deformation and damage behaviour during SPCT are not considered at all. Based on the Chakrabarty membrane theory and utilizing a series of FE creep damage analyses, empirical relations have been proposed in the literature to improve the description of SPCT and to acquire information about creep strain in SPCTs (e.g., (Yang and Wang, 2003; Li and Šturm, 2006)). For instance, Yang and Wang (Yang and Wang, 2003) proposed an empirical relation between the central effective creep strain and the central displacement. Li and Sturm (Li and Šturm, 2006) derived a third order polynomial correlation between the equivalent creep strain at contact edge and the central displacement. However, the application of these empirical correlations is only limited to specific SPCT geometries. In practice, a more generalised approach applicable for any SPCT geometry becomes more desirable. Hyde and Sun et al. (T.H Hyde et al., 2010) proposed a simplified cone model to estimate the 'general' strain levels and membrane stresses in an SPT specimen. In their model (T.H Hyde et al., 2010), a uniform specimen thickness reduction is assumed during deformation along the radial direction. Based on the model by Hyde and Sun et al., Yang et al. (Yang et al., 2017) proposed a hybrid spherical and cone model to take into account the different deformation behaviour observed in the contact and unsupported regions of the specimen. In addition, Zhao et al. (L. Zhao et al., 2019) recently proposed a modified cone model to represent the deformation of the SPCT specimen by considering the variation of the specimen thickness over three regions. Although the aforementioned models (T.H Hyde et al., 2010; Yang and Wang, 2003; Li and Šturm, 2006; Yang et al., 2017; L. Zhao et al., 2019)

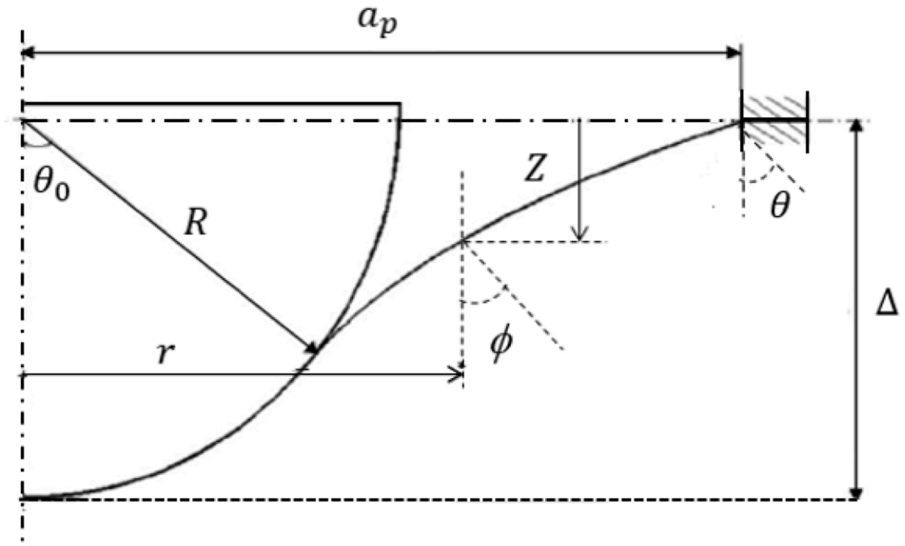

Fig. 2. A schematic illustration of Chakrabarty's membrane stretching model (Chakrabarty, 1970).

have provided useful insights into the SPCT behaviour and improved SPCT data interpretation in relation to the uniaxial creep behaviour, the material response is assumed to be purely geometrical dependant, and therefore, the effects induced by creep damage during SPCT are not constitutively captured. Due to this reason, analytical solutions utilizing creep damage constitutive equations are required to provide a more accurate theoretical representation of the complex deformation mechanism of the small punch creep problem. To the authors' best knowledge, a mechanistic based creep damage analytical solutions for the small punch creep problem is still lacking. In this study, a membrane-based creep damage theory is developed to address such limitations.

The paper is organised as follows: Section 2 provides a brief theoretical background to the problem by introducing the governing equations and main hypothesis including those relevant to the membrane theory and creep continuum damage mechanics (CDM). In Section 3, analytical solutions are presented for the equivalent stress-strain and creep damage at the contact boundary on the basis of Liu-Murakami CDM and membrane theory. In addition, strain energy based analytical solutions are obtained for the small punch creep curve and minimum displacement rate in the SPCT. In Section 4, the capability of the analytical solutions is carefully examined and evaluated via FE creep damage analyses. Section 5 provides a discussion on the key merits and potential applications of the theory. Finally, some concluding remarks are given with indications for further studies.

2. Underlying theory

This section provides a theoretical background into the membrane theory and creep damage mechanics constitutive model, which will form the basis for the analytical derivations presented later in Section 3. In Section 2.1, Chakrabarty's membrane theory is introduced, and the main hypothesis adopted in the analysis are clarified. Besides, the fundamental equations in the membrane theory are outlined. Section 2.2 presents the creep damage mechanics-based model, which is adopted in this work to characterise the creep deformation and damage evolution of the material.

2.1. Membrane theory

2.1.1. Assumptions

Chakrabarty's membrane theory presents an analysis for the stretch forming of a circular metal sheet of a uniform thickness, T_0, deformed by forcing a rigid hemispherical punch head (Chakrabarty, 1970). Fig. 2 shows schematically the geometry of the membrane stretching model. The theory provides a comprehensive description of the stress and strain distribution in a thin disc under membrane deformation mode, and therefore, has been widely utilized for SPCT data interpretation and correlation (CEN 2006; Yang and Wang, 2003; Li and Šturm, 2006). Analytical solutions to this problem are complicated by the moving contact edges between the punch and the disk in addition to the non-linear friction effects. To simplify the analysis, some assumptions were made. The material is assumed to be isotropic, and the punch head is assumed to be well lubricated to neglect any friction effects between the blank and the punch. Further, a rigid plastic material model is adopted in view of the large deformations encountered in the problem (Chakrabarty, 1970). To ensure the applicability of the membrane deformation assumption, the blank thickness is assumed to be sufficiently small compared with the punch radius. Although Chakrabarty's solution is strictly valid for a special material with an exponential hardening law, it can provide a good approximation for real materials exhibiting various hardening laws.

2.1.2. Geometric relationships

In this section, the key geometrical relationships, which are adopted to define the deformation along the blank, are outlined. As shown in Fig. 2, any generic point along the blank can be described by two coordinates (r,z),where for a given point on the blank, r is the current radius; z is the vertical height. Alternatively, the position of a given point can be defined by the meridional angle ϕ, which is the angle between the vertical line and the surface normal. For the contact region, the current radius, r, is related to the meridional angle (ϕ), defined by the range $0 \le \phi \le \theta_0$, through the following relation:

$$r = Rsin\phi \tag{1}$$

where R is the punch radius, and θ_0 is the contact angle, as defined in Fig. 2. In Eq. (1), the current radius, r, is bounded by the range, $0 \le r \le Rsin\theta_0$ while for the unsupported region of the blank, $\theta \le \phi \le \theta_0$, the current radius, r, is defined by Eq. (2), applicable over the range $Rsin\theta_0 \le r \le a_p$:

$$\frac{r}{a_p} = \frac{\sin\theta}{\sin\phi} \tag{2}$$

where a_p is the receiving hole radius; θ denotes the angle at the contact boundary, as defined in Fig. 2, which can be related to the contact angle, θ_0, by the following relationship:

$$\sin\theta = \frac{R}{a_p} sin^2\theta_0 \tag{3}$$

2.1.3. Equilibrium equations

In the absence of friction, the meridional equilibrium in the contact and unsupported regions of the blank is given by Eq. (4) (Chakrabarty, 1970):

$$\frac{\partial(T\ \sigma_r)}{\partial r} = \frac{T}{r}\ (\sigma_c - \sigma_r) \tag{4}$$

while the normal equilibrium equations in the contact and unsupported regions of the blank are given by Eqs. (5.a) and (5.b), respectively:

$$T(\sigma_c + \sigma_r) = pR \tag{5.a}$$

$$\frac{\sigma_c}{\rho_c} + \frac{\sigma_r}{\rho_r} = 0 \tag{5.b}$$

where T is the current blank thickness; σ_c and σ_r represent the circumferential and meridional stresses, respectively; p is the contact pressure. ρ_c and ρ_r are the principal radii of curvature, defined by Eqs. (6.a) and (6.b), respectively:

$$\rho_c = rcosec\ \phi \tag{6.a}$$

$$\rho_r = \frac{\partial r}{\partial \phi}\sec\phi \tag{6.b}$$

The equilibrium equations stated above are valid regardless of the constitutive material model employed.

2.2. Creep damage constitutive equations

Continuum Damage Mechanics (CDM) offers a complementary approach to fracture mechanics for the analysis of creep damage and cracking. CDM based models typically use a scalar variable to represent damage level in the material, with a value ranging from 0 to 1, corresponding to no damage state and full damage state, respectively. The Liu-Murakami CDM (Liu and Murakami, 1998) was proposed to address the strain and damage rates singularities encountered in the classical Kachanov-Robontov CDM (Kachanov, 1958; Rabotnov, 1969) when the damage value approaches unity. The constitutive material model consists of coupled creep and damage equations, which are developed by extending the micromechanics-based constitutive relations of Hutchinson (Hutchinson, 1983) and Riedel (Riedel, 1987) for materials undergoing creep-constrained grain boundaries cavitation. The coupling of creep damage and creep strain within the CDM framework is also supported by microstructural observations on the creep response of metals and alloys at elevated temperatures (Kassner and Hayes, 2003; Abstoss et al., 2019; Ragab et al., 2022; Kachanov, 1986). The capability of the Liu-Murakami model to simulate creep damage and crack growth in high-temperature materials was examined in previous work (T.H. Hyde et al., 2010). The model incorporates a microcrack parameter, ρ, which is dependant on the stress exponent, n, as described below:

$$\rho = \frac{2(n+1)}{\pi\sqrt{1+3/n}}\omega^{3/2} \tag{7}$$

The multi-axial form of the creep strain rate is given by Eq. (8), which incorporates the effects of both the damage and stress state on

the evolution of creep deformation.

$$\dot{\varepsilon}_{ij}^{c} = \frac{3}{2} A \sigma_{eq}^{n-1} S_{ij} \exp\left(\frac{2(n+1)}{\pi\sqrt{1+3/n}} \left(\frac{\sigma_1}{\sigma_{eq}}\right)^2 \omega^{3/2} \right) \tag{8}$$

The stress-based creep damage evolution is defined by:

$$\frac{d\omega}{dt} = B\left[\frac{1-\exp(-q_2)}{q_2}\right] \sigma_{Rup}^{\chi} \exp(q_2 \omega) \tag{9}$$

where S_{ij} and $\dot{\varepsilon}_{ij}^{c}$, (i, j = 1,2,3) are the deviatoric stress and creep rate deformation tensors, respectively; σ_{eq}, σ_1 and σ_{Rup} are the equivalent, maximum principal and rupture stresses, respectively; ω is a state variable , $\omega \in [0,1]$; A, n, B, χ, q_2 are the material constants obtained via uniaxial tensile creep tests.

The creep rupture stress in Eq. (9) is assumed to be a combination of the maximum principal stress and the von-Mises equivalent stress as given below:

$$\sigma_{Rup} = \alpha\sigma_1 + (1-\alpha)\sigma_{eq} \tag{10}$$

where α is a material constant characterising the material behaviour under the multi-axial stress states. The value of this parameter can be identified from notched bar creep rupture tests in conjunction with FE creep damage simulations (Ragab et al., 2021). It should be noted that there are numerous parameters characterising the multiaxial creep that generally depend on the type of continuum damage mechanics material model employed (i.e., whether a stress-based or strain-based CDM). In stress based CDM, the multi-axial creep behaviour is typically characterised by the multi-axial factor, α, while in strain-based damage models, stress triaxiality and lode parameter are often used to define the stress state (Ragab et al., 2022).

3. Analytical solutions

In this section, membrane stretching-based creep damage analytical solutions are derived which are extremely useful in representing the deformation and failure behaviour in small punch creep tests. These solutions present the key relationships between contact angle, creep deformation, stresses, damage and rupture life. In Section 3.1, analytical solutions are derived to mathematically represent the stresses in the SPCT. Section 3.2 presents analytical solutions of creep damage and creep failure life for the small punch creep problem. In Section 3.3, the equivalent creep strain at contact edge is obtained. Strain energy-based solutions are derived in Section 3.4 for the small punch creep curve and minimum displacement rate. Throughout this paper, the stress is measured by Cauchy stress while the creep deformation is measured by the rate of deformation or Almansi strain.

3.1. Stress solution

From the membrane stretching theory, in the absence of friction, the stress state can be considered as balanced bi-axial tension, as given below:

$$\sigma_c = \sigma_r \tag{11}$$

where σ_c and σ_r are the circumferential and meridional stresses, respectively.

Since no shear stresses are acting, the principal stresses can be defined by Eqs. (12.a) and (12.b):

$$\sigma_1 = \frac{\sigma_c + \sigma_r}{2} + \sqrt{\left(\frac{\sigma_c - \sigma_r}{2}\right)^2 + 0} = \sigma_c \tag{12.a}$$

$$\sigma_2 = \frac{\sigma_c + \sigma_r}{2} - \sqrt{\left(\frac{\sigma_c - \sigma_r}{2}\right)^2 + 0} = \sigma_r \tag{12.b}$$

Consequently, the von Mises equivalent stress component can be obtained by:

$$\sigma_{eq} = \sqrt{\frac{(\sigma_1-\sigma_2)^2 + (\sigma_1-\sigma_3)^2 + (\sigma_2-\sigma_3)^2}{2}} = \sigma_c = \sigma_r \tag{13}$$

Hence, regardless of the value taken for the multi-axiality parameter, α, the rupture stress can be re-written as:

$$\sigma_{Rup} = \sigma_{eq} = \sigma_c \tag{14}$$

From the normal equilibrium (i.e., Eq. (5.a)), and based on Eqs. (11-14), the rupture stress can be defined as follows:

$$\sigma_{Rup=} \frac{pR}{2T} \tag{15}$$

A uniform thickness reduction is proposed along the radial direction (during the primary and secondary creep stages) based on

Chakrabarty's membrane theory as follow:

$$T = T_0\left(\frac{1+cos\theta_0}{1+cos\theta}\right)^2 \tag{16.a}$$

where T and T_0 are the current and initial blank thickness, respectively.

In order to account for the localised thinning occurring within the latest stages of the test (tertiary creep), the current thickness at any given point within the contact region (i.e., $0 \le \phi \le \theta_0$) may be defined by:

$$T = T_0\left[\frac{(1+cos\theta_0)^4}{(1+cos\phi)^2(1+cos\theta)^2}\right] \tag{16.b}$$

while the variation of the thickness in the unsupported region during the tertiary creep may be assumed to follow Eq. (16.a).

The trigonometric term, $cos\theta$, in Equation (16), is related to the contact angle through the following:

$$cos\theta = \sqrt{1-\left(R/a_p\right)^2 sin^4\theta_0} \tag{17}$$

On this basis, the equivalent stress at any given point within the contact region ($0 \le r \le Rsin\theta_0$) and at a given test instance can be determined from Eq. (15) (normal equilibrium) if the current thickness and the contact pressure at that point are known. Similarly, the stress distribution in the radial direction of the unsupported region ($Rsin\theta_0 \le r \le a_p$) can be determined from the meridional equilibrium by solving Eq. (4), which can be simplified under friction free conditions as: $\frac{\partial(T\ \sigma_r)}{\partial r} = 0$

Based on Eq. (15), the equivalent stress at the contact edge can be expressed in terms of the punch load as:

$$\sigma_{eq} = \frac{F}{2\pi RTsin^2\theta_0} \tag{18}$$

where θ_0 and F are the contact angle and the punch force, respectively.

The evolution of the thickness at the contact edge can be obtained from Equation (16).

Substituting Equations (16) and (17) into Eq. (18) yield the following:

$$\sigma_{Rup} = \sigma_{eq} = \frac{F}{2\pi RT_0}\left(\frac{1+\sqrt{1-\left(R/a_p\right)^2 sin^4\theta_0}}{sin\theta_0+\frac{1}{2}sin2\theta_0}\right)^2 \tag{19}$$

Remark 1

It is worth noting that, during the early stages of creep deformation, the membrane based analytical solution breaks down, predicting infinite stress values, as shown by Eq. (20). Such singularity can be attributed to bending deformations, which possibly govern the small punch creep response during the early stages.

$$\lim_{\theta_0 \to 0} \frac{F}{2\pi RT_0}\left(\frac{1+\sqrt{1-\left(R/a_p\right)^2 sin^4\theta_0}}{sin\theta_0+\frac{1}{2}sin2\theta_0}\right)^2 = \infty \tag{20}$$

3.2. Creep damage evolution and failure life

Since the contact angle θ_0 is a monotonically increasing parameter, it can be taken as a time scale and therefore the damage evolution in Eq. (9) can be re-defined in terms of the contact angle. To represent the evolution of contact angle with respect to time, a power law is proposed based on FE analysis, as described below:

$$\frac{\theta_0}{\theta_{0f}} = \beta\left(\frac{t}{t_f}\right)^m \tag{21}$$

with $0 < \theta_0 < \theta_{0f}$; $0 < t < t_f$. where θ_{0f} and t_f represent contact angle at failure and creep rupture life, respectively; β and m are constants.

Based on Eq. (21), the following derivative can be obtained:

$$dt = \frac{t_f}{m}\left(\frac{1}{\beta\ \theta_{0f}}\right)^{1/m}\theta_0^{\frac{1-m}{m}}d\theta_0 \tag{22}$$

Substituting Eqs. (19, 21, 22) into Eq. (9) yield an expression for the creep damage at the contact edge as follows:

$$\int \exp(-q_2\omega)d\omega = \int B\left[\frac{1-\exp(-q_2)}{q_2}\right]\left(\frac{F}{2\pi RT_0}\left(\frac{1+\sqrt{1-\left(\frac{R}{a_p}\right)^2 sin^4\theta_0}}{sin\theta_0+\frac{1}{2}sin2\theta_0}\right)^2\right)^{\chi}\frac{t_f}{m}\left(\frac{1}{\beta\ \theta_{0f}}\right)^{1/m}\theta_0^{\frac{1-m}{m}}d\theta_0 \tag{23}$$

If the contact angle at failure is known, creep rupture life, t_f, under a given punch force, F, can also be identified from the following definite integral with the damage ω changing from 0 to 1, corresponding to no damage and full damage states, respectively.

$$t_f = \frac{m\ (2\pi RT_0/F)^{\chi}\ \left(\beta\ \theta_{0f}\right)^{1/m}}{B\int_0^{\theta_{0f}}\left(\left(\frac{1+\sqrt{1-\left(R/a_p\right)^2 sin^4\theta_0}}{sin\theta_0+\frac{1}{2}sin2\theta_0}\right)^2\right)^{\chi}\theta_0^{\frac{1-m}{m}}d\theta_0} \tag{24}$$

Remark 2

It can be shown that Eq. (24) can be reduced into the following forms:

$$t_f \propto \left(\frac{1}{F}\right)^{\chi} \tag{25.a}$$

$$\log\ t_f\ = \log\ C - \chi\ logF \tag{25.b}$$

where C is a constant accounting for the proportionality between punch loading and the respective creep rupture life.

On the basis of Eq. (25.b), one can see the linear relationship (on logarithmic scale) between creep rupture lives and the punch loading applied in the SPCT. Such correlation has been confirmed experimentally as well for various materials at high temperatures (e.g., refs (Cortellino et al., 2017; L. Zhao et al., 2019)).

3.3. Equivalent creep strain

Creep equivalent strain rate under equal biaxial stress state conditions can be reduced into the following equation:

$$\dot{\varepsilon}_{eq} = A\sigma_{eq}^n \exp\left(\frac{2(n+1)}{\pi\sqrt{1+3/n}}\omega^{3/2}\right) \tag{26}$$

Since the adopted constitutive material model consists of coupled creep strain and creep damage equations, the evaluation of the effective creep strain component at the contact edge, for instance, requires use of Eq. (23) for creep damage evolution. The equivalent stress under membrane deformation mode can be evaluated from Eq. (19).

A close form analytical solution may not be readily obtained from Eq. (26). Instead, the equivalent creep strain at contact edge is obtained using a time marching procedure.

3.4. Analytical derivations of small punch displacement and minimum displacement rate

In this section, strain energy-based analytical solutions are derived for the small punch displacement-time behaviour and minimum displacement rate on the basis of the Liu-Murakami CDM and the membrane stretching theory. The strain energy formulations for the contact region and unsupported region are shown in Section 3.4.1. Using the balance of external and internal energies, the punch displacement-time response of the disc is solved accordingly as given in Section 3.4.2. Finally, a simplified, approximate model for the minimum displacement rate is proposed in Section 3.4.3.

3.4.1. Strain energy formulations

The displacement rate can be calculated by the complementary strain energy method. The strain energy density per unit volume, w_d, of the thin disc due to creep loading can be evaluated as:

$$w_d(t) = \int_0^t \sigma_{eq}\dot{\varepsilon}_{eq}\ dt \tag{27}$$

Note that since we are dealing with large deformations, it is reasonable to neglect the contribution of the elastic deformation. The internal work over the entire effective material volume can be represented by:

$$W_{in} = \iiint \odot \mathrm{w_d}\ \mathrm{dv} \tag{28}$$

Now, consider an infinitesimally small element in the contact region whose volume dv is given by:

$$dv = TdA_c \tag{29}$$

with T being the current thickness and dA_c is the change in surface area of the contact region during creep.

For a circular disc, the contact area between the punch and the disc, and the change in the contact area can be reasonably evaluated by Eqs. (30.a) and (30.b), respectively.

$$A_c = \pi r^2 \tag{30.a}$$

$$dA_c = 2\pi r dr \tag{30.b}$$

where for the contact region, the current radius, r, is as dfined by Eq. (1), i.e., r is bounded by the range $0 \le r \le R sin\,\theta_0$.

Based on Eqs. (27-30) and assuming that the change in the effective stress along the disc thickness is insignificant (i.e., $\frac{\partial \sigma_{eq}}{\partial T} \approx 0$), an expression for the internal work done over the contact region can be obtained as below:

$$W_{in,c} = \pi R^2 A \int_0^{t_f} \int_0^{\theta_0} \sigma_{eq}^{n+1} \exp\left(\frac{2(n+1)}{\pi\sqrt{1+\frac{3}{n}}}\,\omega^{3/2}\right) T \sin 2\phi d\phi d\phi dt \tag{31}$$

where A, n are the creep constants in the Liu-Murakami CDM; σ_{eq}, ω define the equivalent stress and creep damage in the contact region, respectively; T is the current thickness.

Using a similar approach, the internal work done over the unsupported region of the blank can be quantified as elaborated below.

The change in the surface area of the unsupported region dA_{us} can be evaluated as:

$$dA_{us} = -2\pi R^2 \, sin^4\theta_0 cosec^2\phi \cot\phi d\phi \tag{32}$$

The internal work done over the unsupported region can be evaluated as follow:

$$W_{in,us} = -2\pi R^2 A \int_0^{t_f} \int_{\theta}^{\theta_0} \sigma_{eq}^{n+1} \exp\left(\frac{2(n+1)}{\pi\sqrt{1+\frac{3}{n}}}\,\omega^{3/2}\right) T sin^4\theta_0 cosec^2\phi \cot\phi d\phi d\phi dt \tag{33}$$

Eq. (33), σ_{eq}, ω are the equivalent stress and creep damage in the unsupported region of the blank, respectively. The other symbols are as defined earlier.

3.4.2. Punch displacement-time solution

The small punch displacement vs time response can be obtained by balancing the external and internal energy in the thin disc as illustrated below.

The net total internal work done on the disc specimen is the sum of internal energies across the contact and unsupported regions, which are defined by Eq. (31) and Eq. (33), respectively.

$$W_{net} = W_{in,\,c} + W_{in,\,us} \tag{34}$$

The external work done by the punch load can be defined as:

$$W_{ext.} = \int_0^t F\dot{\Delta}\, dt \tag{35}$$

where F and $\dot{\Delta}$are the punch load and displacement rate, respectively.

Based on Eq. (34) and Eq. (35), an expression for the displacement rate can be derived as follow:

$$\dot{\Delta} = \frac{\pi R^2 A}{F}\left[\int_0^{\theta_0} \sigma_{eq}^{n+1} \exp\left(\frac{2(n+1)}{\pi\sqrt{1+\frac{3}{n}}}\,\omega^{3/2}\right) T \sin 2\phi d\phi + 2\int_{\theta_0}^{\theta} \sigma_{eq}^{n+1} \exp\left(\frac{2(n+1)}{\pi\sqrt{1+\frac{3}{n}}}\,\omega^{\frac{3}{2}}\right) T sin^4\theta_0 cosec^2\phi \cot\phi d\phi d\phi\right] \tag{36}$$

A closed form solution cannot be readily obtained from Eq. (36). Hence, the punch displacement, Δ, may be obtained using numerical techniques as follow:

$$\Delta_i = \Delta_{i-1} + \dot{\Delta}_i \Delta t \tag{37}$$

where Δt is the time step.

3.4.3. Minimum displacement rate

During secondary creep regime, Liu-Murakami CDM, can be reduced to Norton type law of the following form by excluding the primary creep term and damage:

$$\dot{\varepsilon}_{eq} = A_1 \sigma_{eq}^{n_1} \tag{38}$$

where A_1, n_1 are secondary creep properties as obtained from conventional uniaxial creep tests.

In what follows, an approximate solution is presented to describe the minimum displacement rate in the SPCT by simplifying Eq. (36) presented in the previous subsection.

It is observed that the effective stress in the SPCT attains a stationary value during the secondary creep stage (Ma et al., 2009; Zhai et al., 2004). To achieve this, the following conditions should be satisfied:

$$\frac{\partial \sigma_{eq}}{\partial \theta_0} = 0 \tag{39}$$

In other words, the trigonometric term $\left(\frac{1+\sqrt{1-(R/a_p)^2 sin^4\theta_0}}{sin\theta_0+\frac{1}{2}sin2\theta_0}\right)^2$ in Eq. (19) should keep a minimum value, yielding the following:

$$\cos\theta_0 + \cos 2\theta_0 + \frac{(R/a_p)^2(2\sin\theta_0 + \sin 2\theta_0)\, sin^3\theta_0 cos\theta_0}{\sqrt{1-(R/a_p)^2 sin^4\theta_0} + \left(1-(R/a_p)^2 sin^4\theta_0\right)} = 0 \tag{40}$$

A close form solution from Eq. (40) may not be readily obtained. Therefore, a general relationship is derived between the contact angle (in radian) at the local minimum point and the ratio $\left(\frac{R}{a_p}\right)^2$ by means of non-linear inverse fitting in MATLAB as follow:

$$\begin{aligned} &\sin\theta_0 = 0.854e^{0.145\left(\frac{R}{a_p}\right)^2} \\ &\text{or} \\ &\theta_0 = sin^{-1}\left[0.854e^{0.145\left(\frac{R}{a_p}\right)^2}\right] \end{aligned} \tag{41}$$

where $0.5 \le \frac{R}{a_p} < 1$.

The total internal work done during the secondary creep can be approximated by the following equation, assuming a uniform thickness reduction during deformation and uniform contact pressure:

$$W_{in} = A_1 \left(\frac{F}{2\pi R T_0}\right)^{n_1+1} \left[\left(\frac{1+\sqrt{1-(R/a_p)^2 sin^4\theta_0}}{sin\theta_0+\frac{1}{2}sin2\theta_0}\right)^2\right]^{n_1+1} (\pi\, a_p{}^2 T_0) \tag{42}$$

By balancing the external and internal work, an approximate solution for the minimum displacement rate can be derived as follow (for a given force and geometry):

$$\dot{\Delta}_{min} = \frac{A_1\, a_p^2}{(2R)^{n_1+1}\,(\pi T_0)^{n_1}} \left[\left(\frac{1+\sqrt{1-(R/a_p)^2 sin^4\theta_0}}{sin\theta_0+\frac{1}{2}sin2\theta_0}\right)^2\right]^{n_1+1} F^{n_1} \tag{43}$$

where the contact angle at the local minimum is related to the ratio (R/a_p) through Eq. (41).

Remark 3

For a given SPCT geometry, (say $R/a_p = 0.52$), a local minimum can be found at $\theta_0 \approx 63^0$, and therefore, the minimum displacement rate can be approximated by the following:

$$\dot{\Delta}_{min} = \frac{A_1\, a_p^2}{(2R)^{n_1+1}\,(\pi T_0)^{n_1}} (2.175)^{n_1+1} F^{n_1} \tag{44}$$

Eq. (44) proves that the minimum displacement rate in an SPCT can be effectively reduced to Norton type law of the following form:

$$\dot{\Delta}_{min} = c_1 F^{n_1} \tag{45.a}$$

where c_1 and n_1 are constants. Experiemntal data from small punch tests have also identified a power law relationship between the minimimum displacement rate and punch loading (Kumar and Laha, 2015; Cortellino et al., 2017), which qualitatively agree with our analytical solution.

Eq. (45.a) can indeed be represented in the following linear form:

$$log\ \dot{\Delta}_{min} = log\ c_1 + n_1 log\ F \tag{45.b}$$

Table 1
Creep damage properties for a P91 steel at 650°C (stress in MPa and time in hours) (Cacciapuoti et al., 2016).

A	n	B	χ	q_2	α
1.092×10^{-20}	8.462	2.952×10^{-16}	6.789	3.2	0.21

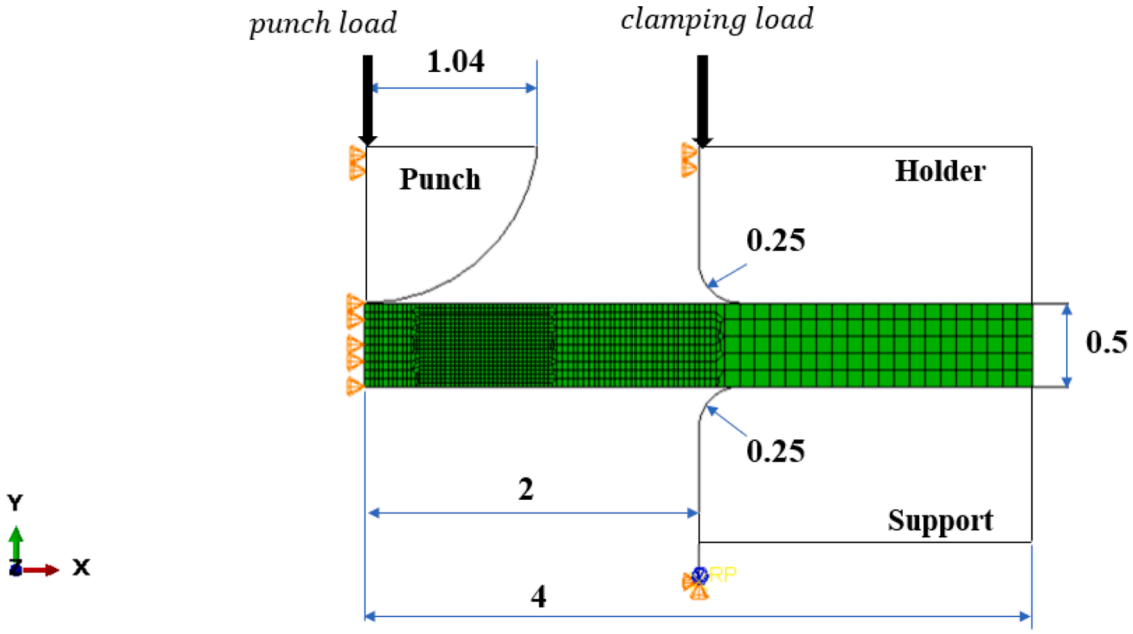

Fig. 3. A schematic illustrating the geometrical details of the small punch creep test setup and the FE model with the mesh scheme, loading and boundary conditions. (NB: All dimensions are in mm).

The theoretical analysis presented here suggests that a correlation can be obtained between the secondary creep properties obtained by the SPCTs and those derived from conventional uniaxial creep tests. Further details on this are provided in Section 5.2.

4. Comparsion with finite element

In this section, the accuracy of the proposed membrane-based solutions will be examined through FE calibration. Details of the FE model are provided in Section 4.1, while the calibration results are presented in Section 4.2.

4.1. Finite element model

A FE creep damage analysis has been performed to study creep deformation and damage in the small punch creep tests and to verify the accuracy of the analytical solutions presented earlier in Section 3. Creep damage constitutive model as defined by Eqs. (8-10) are implemented into a user defined subroutine in the FE software ABAQUS (ABAQUS 2019) with the material parameters relevant to the creep constitutive model are as listed in Table 1. Typically, the uniaxial creep parameters ($A,\ n,\ B, \chi, q_2$) are identified from uniaxial creep tests while the triaxiality parameter, α, is derived based on multi-axial notched bar creep tests.

The small punch creep test setup and its geometrical details are as illustrated in Fig. 3, (Specimen diameter = 8 mm, specimen thickness = 0.5 mm, receiving hole radius = 2 mm, punch radius =1.04 mm). Taking an advantage of the problem axial symmetry, only half of the geometry was modelled using bilinear axisymmetric 4-node elements with reduced integration (designated as CAX4R in the FE Software ABAQUS). The developed FE consists of 1186 elements, with a finer mesh discretization applied to the region near the contact boundary between the specimen and the punch where the stress and strain fields are expected to vary rapidly. The punch, holder and supporting dies were modelled as rigid bodies, while the specimen was considered as the only deformable solid in the FE model. The FE analysis was performed under frictionless contact conditions to comply with the theoretical hypothesis adopted in Section 2 for the membrane-based solution. Surface to surface contact interactions were assigned for all of the contacting pairs. The imposed loadings and boundary conditions in the FE model are demonstrated in Fig. 3. The analysis was conducted under different punch loading levels ranging from 130 to 150 N. A clamping load of 500 N was applied on the reference point of the upper die (holder) to tighten the specimen between the two dies. The radial and axial displacements and the rotation around the axis of symmetry of the lower clamp were constrained. In addition, the horizontal displacement and the rotation of the punch and the upper clamp were constrained. Axisymmetric boundary conditions were applied on the left side of the specimen as shown in Fig. 3. Large deformation

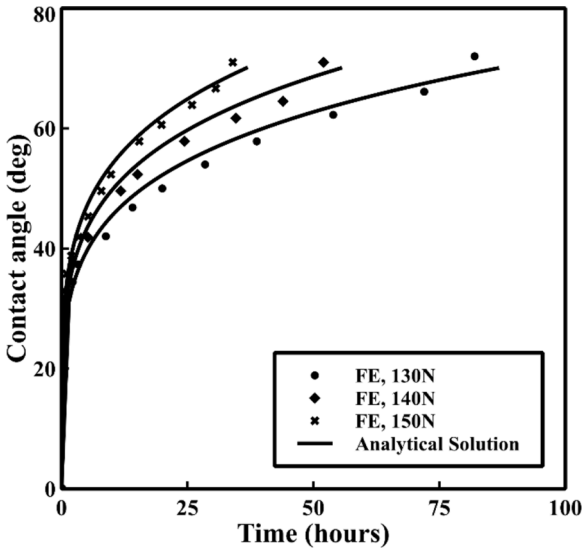

Fig. 4. Comparison between the analytical and FE solutions of contact angle evolution vs time for a SPCT for a P91 steel at 650°C and under 130–150 N punch loadings.

effects were considered in the FE analysis through the application of the geometrical non-linearity formulation available in ABAQUS.

4.2. Finite element results

The results extracted from the FE analysis will be utilized in the validation process of the analytical solutions as further elaborated in the following sub-sections.

4.2.1. Contact angle evolution

In Section 3, an expression describing the monotonic increase of contact angle with respect to time has been derived, as shown by Eq. (21). To evaluate the accuracy of the proposed solution, the analytical predictions obtained from the proposed model are compared with the corresponding FE results as illustrated in Fig. 4. As shown, the theoretical model reasonably predicts the evolution of contact angle in the SPCT under the given punch loadings.

4.2.2. Equivalent stress and strain

The evolution of effective membrane stress during creep at contact edge region can be analytically evaluated in the time domain on the basis of Eq. (19) and Eq. (21). The equivalent stress at contact edge is evaluated for the SPCT geometry illustrated in Fig. 3, and under punch loadings within the range 130–150 N. The analytical predictions are then compared with those acquired from the FE creep damage analysis and the results are shown in Fig. 5. In general, the analytical solutions successfully capture stress redistribution occurring during creep loading in a satisfactory agreement with the FE predictions. However, it may be noted that the membrane-based solution breaks down during the very early stages of creep deformation (i.e., the analytically predicted stress values tend to infinity, in line with Eq. (20)). This singularity can be related to the possible, prevalent bending deformation effects in the early stage of creep, which have not been included in the present analytical solutions.

Fig. 6 compares the analytical creep equivalent strain patterns at contact edge with the corresponding FE results for an SPCT under 130–150 N punch loadings. Since the evaluation of the effective creep strain component depends on the equivalent stress and creep damage, the analytical values for the creep equivalent strain at contact edge were determined following the procedure described in Section 3.3. It can be seen that the analytical solution exhibits the characteristics of creep deformation at various load levels, and the three conventional creep stages (primary, secondary and tertiary creep) are successfully re-produced in an excellent agreement with the FE predictions. As the load increases from 130 N to 150 N, the minimum creep rate increases, and creep rupture life shortens.

The distributions of the equivalent stress and equivalent creep strain in the radial direction within the contact region, $0 \leq r \leq R\sin\theta_0$, at failure are shown in Fig. 7a and Fig. 7b, respectively. Assuming uniform contact pressure, the equivalent stress at any point, r, may be determined following the procedure demonstrated in Section 3.1. Consequently, the equivalent creep strain at any given point in the radial direction can be determined from the rate of deformation by implementing Eq. (26) in Section 3.3.

4.2.3. Creep damage evolution and failure life evaluation

The evaluation of creep damage and creep life for the SPCT is of great engineering significance. Creep damage evolution at contact edge of a small punch specimen can be analytically defined by Eq. (23). To demonstrate the accuracy of our solution, the theoretical predictions of creep damage for a SPCT specimen under 130–150 N punch loading are compared with the FE results in Fig. 8a. As

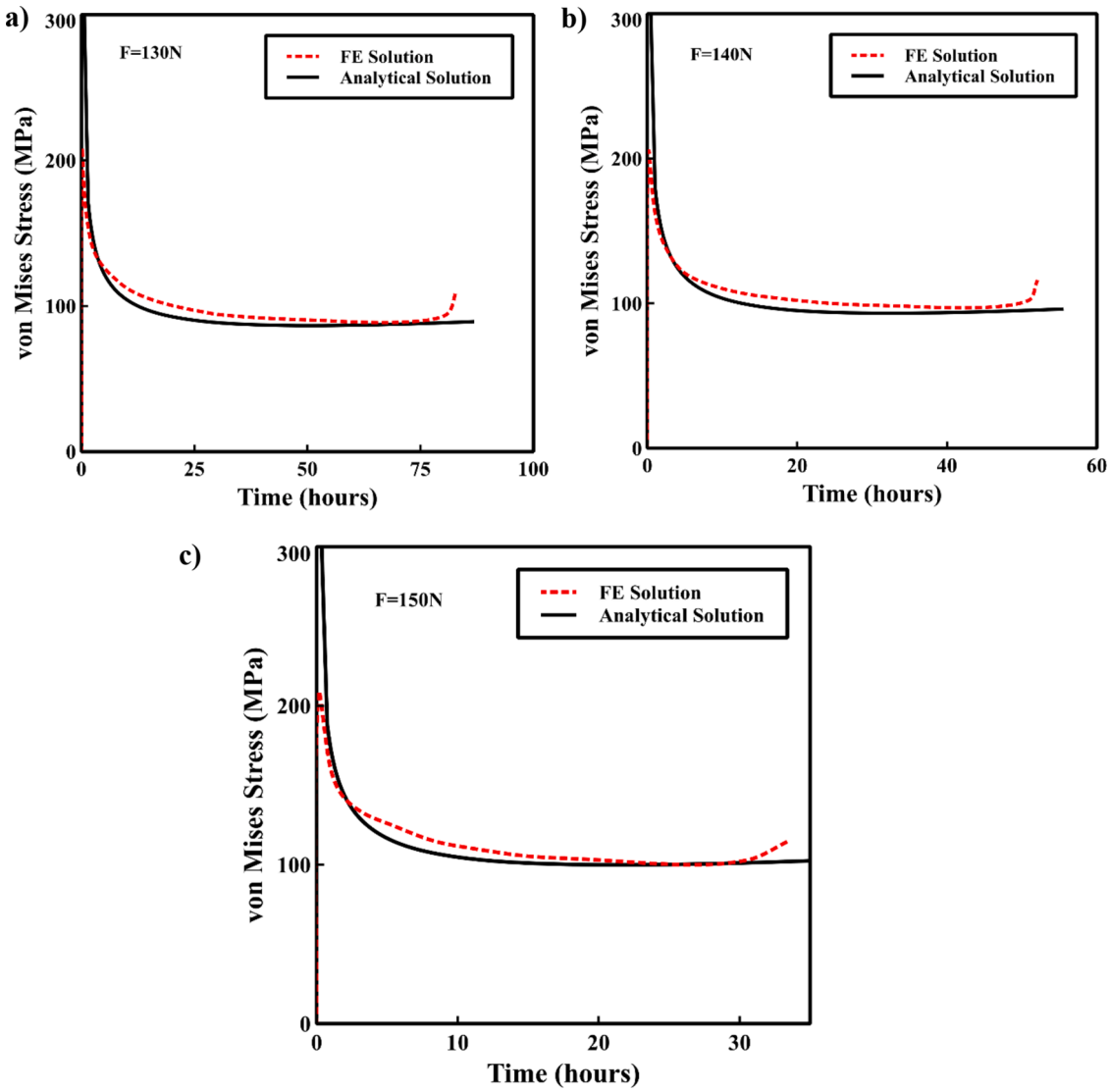

Fig. 5. Comparison between the analytical and FE solutions of von Mises equivalent stress vs time at contact edge of a SPCT for a P91 steel at 650°C and under punch loadings of a) $F = 130$ N, b) $F = 140$ N, and c) $F = 150$ N.

shown, both the analytical and FE creep damage curves are in good agreement. Creep rupture life under a given punch force, F, can be evaluated analytically on the basis of Eq. (24). An excellent agreement is obtained between the analytical and FE predictions, as demonstrated in Fig. 8b. Further, both the analytical and FE results exhibit linear trends on a logarithmic scale, which is consistent with the proposed solution, Eq. (25.b).

4.2.4. *Punch displacement-time solutions*

The punch displacement-time curve constitutes a primary output of the small punch creep test. In the present study, energy-based analytical solutions are proposed to represent the punch-displacement time behaviour under a given punch force and SPCT geometry, as given by Eq. (36) and Eq. (37) in Section 3 (i.e., the deformations in this case are governed by form of creep damage constitutive model). The results obtained from the analytical solutions compare favourably with the corresponding FE data as shown in Fig. 9. In addition, the three typical stages corresponding to the primary, secondary and tertiary creep in small punch creep tests are reasonably predicted by the analytical theory. The regions where the FE results deviate from the membrane-based analytical solutions are those where the deformations are not purely membrane dominated (i.e., bending effects are expected to interplay).

4.2.5. *Minimum displacement rate*

A key parameter that can be extracted from the displacement-time curves is the minimum displacement rate, which is of engineering significance due to its incorporation in the commonly adopted empirical based approaches such as Monkman-Grant relation

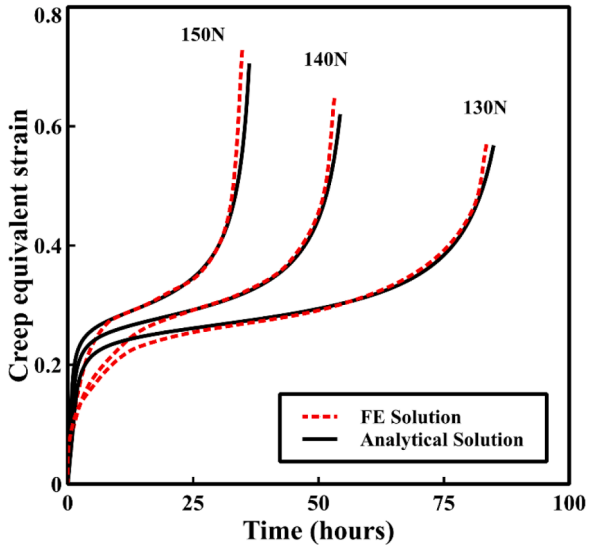

Fig. 6. Comparison between the analytical and FE solutions of von Mises equivalent creep strain (CEEQ) vs time at contact edge of SPCTs for a P91 steel at 650°C and under 130–150 N punch loadings. (Specimen geometries are as clarified in Fig. 3).

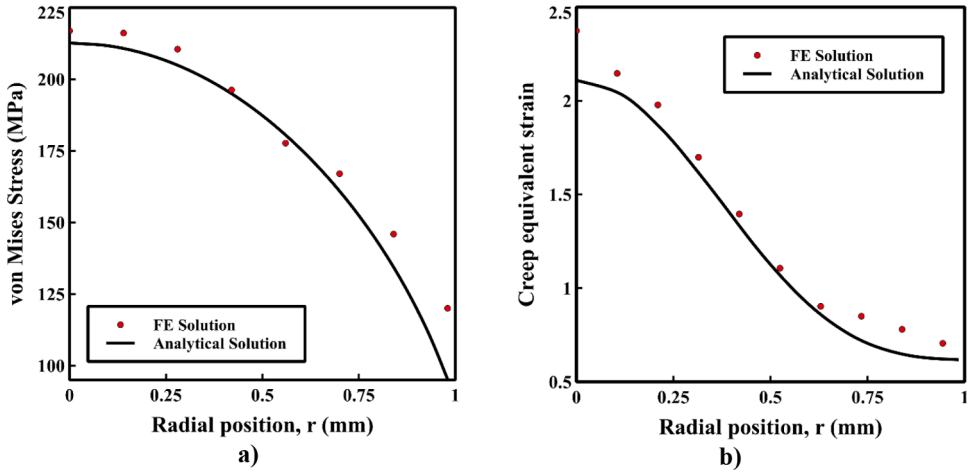

Fig. 7. Comparison between the analytical and FE distributions of a) von Mises equivalent stress and b) Creep Equivalent strain along the radial direction of the contact region ($0 \leq r \leq R\sin\theta_0$) at failure for a P91 SPCT at 650°C and under punch loading of 140 N. .

for creep rupture lives estimation. An approximate theoretical solution has been derived using a simplified power law (Norton's law) to evaluate the minimum displacement rate in SPCT, as demonstrated in Section 3.4.3. The proposed solution is calibrated against the results obtained from FE steady state analysis, with the relevant steady state creep properties of Norton's law adopted in the analysis being: ($A_1 = 1.092 \times 10^{-20}$; $n_1 = 8.462$). It should be noted that in the steady state analysis, the effects of creep damage on the minimum creep rate are excluded. As shown in Fig. 10, the analytical solution yields very reasonable results compared with those derived from the FE steady state analyses. Further, a linear correlation is present between the minimum displacement rate and the applied punch loading (on logarithmic scale), which is in agreement with Eq. (45.b). Another key benefit from the present solutions is the capability to directly correlate the uniaxial secondary creep properties (A_1, n_1) to small punch creep tests data on analytical basis. This will be further discussed in Section 5.2.

5. Discussion and conclusions

In this section, the analytical results from our theoretical model are compared with other existing analytical solutions in the literature, as illustrated in Section 5.1. Further, some important applications of the proposed theory for determining the power law creep parameters have been emphasised, utilizing experimental data as elaborated in Section 5.2. Finally, concluding remarks are provided in Section 5.3.

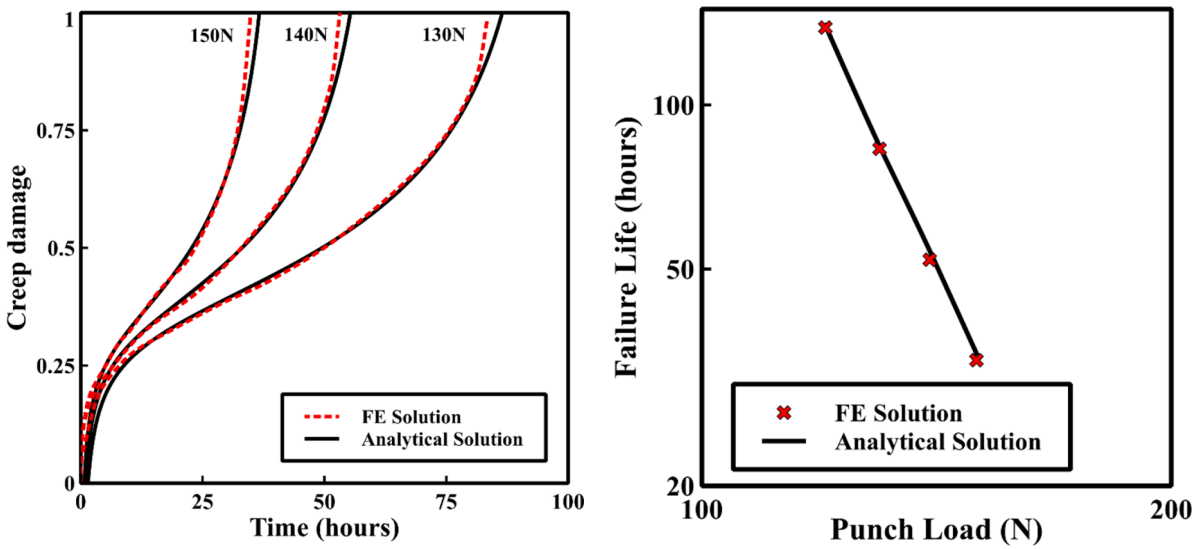

Fig. 8. **a**: Comparison between the analytical and solutions of creep damage evolution at contact edge of SPCTs for a P91 steel at 650°C and under 130–150 N punch loadings. (Specimen geometries are as clarified in Fig. 3). Fig.8b: Logarithmic plot comparing the analytical and FE solutions of creep rupture lives of SPCTs for a P91 steel at 650°C and under 120–150 punch loading.

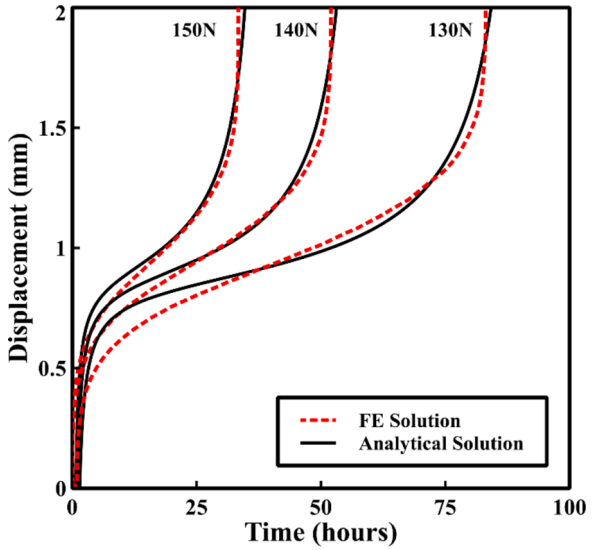

Fig. 9. Comparison between the analytical and FE solutions of punch displacement-time curves of SPCTs for a P91 steel at 650°C and under 130–150 N punch loading.

5.1. Comparison with existing analytical solutions

In Section 4, the predictive capability of our membrane stretching based analytical solutions was examined by comparing them with the FE creep damage analysis. It was shown that the proposed solutions accurately represent the local stresses, damage, contact angle and full stage creep deformation of the small punch creep test. To further demonstrate the powerfulness of the proposed solutions, our membrane-based creep damage analytical solutions are compared with the existing solutions in the literature, namely those proposed by Chakrabarty (Chakrabarty, 1970) and by Hyde and Sun et al. (T.H Hyde et al., 2010). The latter solutions are simplified geometrical relations characterising the local stresses and deformation in SPCTs. Thus far, those relations have been commonly adopted for SPCT data interpretation (CEN 2006; T.H Hyde et al., 2010) for their simplicity. The fundamental difference between our solutions and the geometrical models outlined above is that the latter do not provide a mechanistic-based description to the small punch creep behaviour, whilst the solutions proposed in this study are governed by creep damage constitutive material model and thus, have a clear physical meaning. As such, the overall prediction of the proposed analytical model is both geometry and material

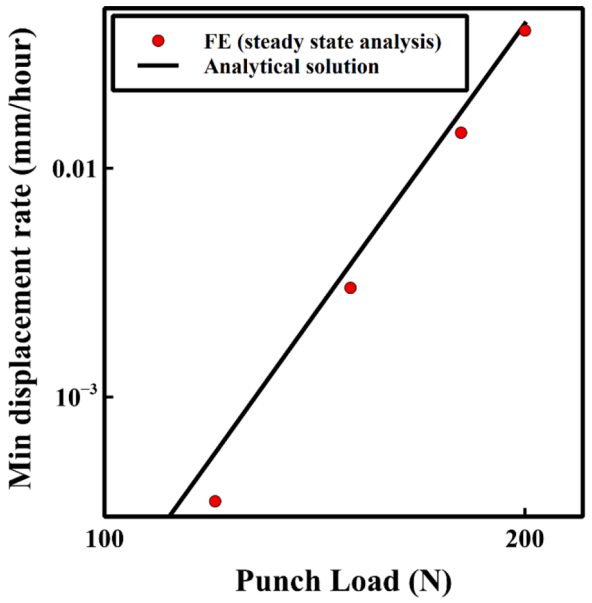

Fig. 10. Comparison between the analytical and FE solutions (under steady state creep) of minimum displacement rate of SPCTs for a P91 steel at 650°C and under 120–200 N punch loading. (Specimen geometries are as clarified in Fig. 3).

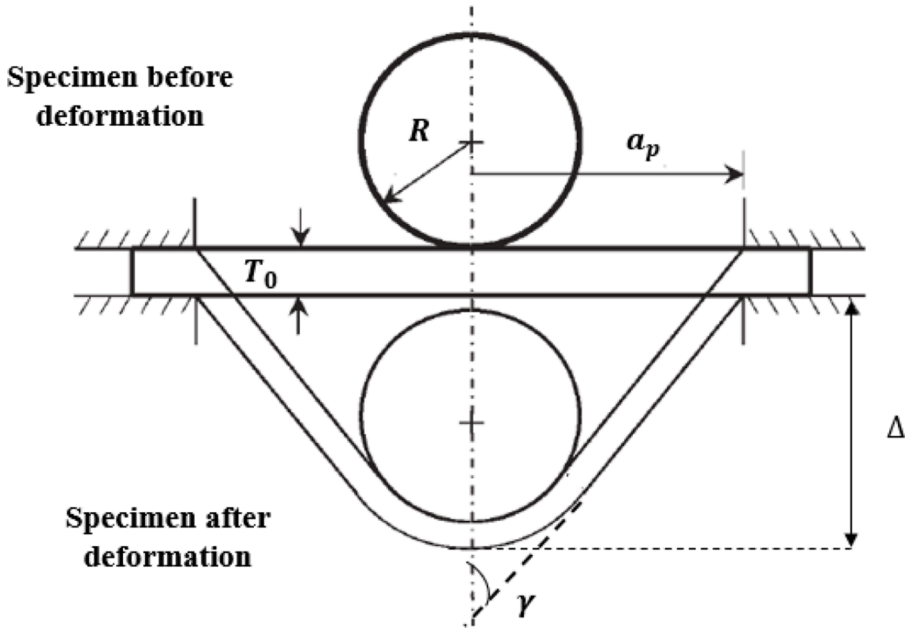

Fig. 11. A schematic illustrating Hyde and Sun et al. cone model (T.H Hyde et al., 2010).

dependant. As discussed earlier, to allow for a succinct mathematical analysis, Chakrabarty's membrane theory (Chakrabarty, 1970) assumes a rigid plastic material model, and the meridional membrane stress at contact edge is defined by Eq. (46), while the evolution of punch displacement at a given contact angle is prescribed by the geometrical relation represented by Eq. (47). Hyde and Sun et al. (T. H Hyde et al., 2010) proposed a simplified cone model, as schematically shown in Fig. 11, for the analysis of SPCTs by assuming a uniform specimen thickness reduction along the radial direction during SPCT deformation. In their model, the evolution of meridional membrane stress at contact edge is given by Eq. (48), while the punch displacement is approximated by Eq. (49).

$$\sigma_{m=} \quad \frac{F}{2\pi RTsin^2\theta_0} \tag{46}$$

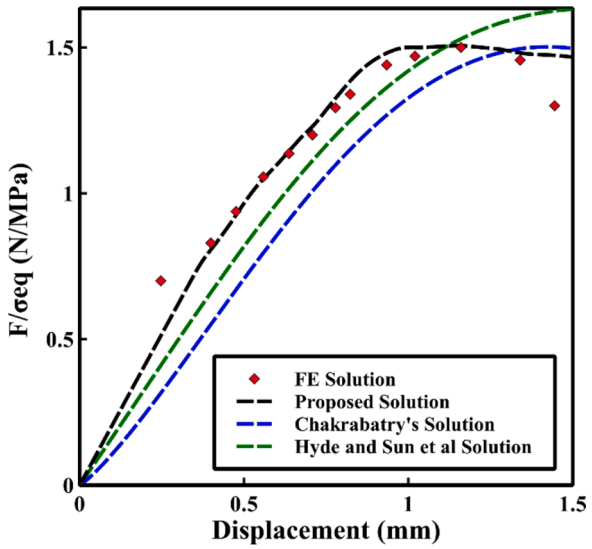

Fig. 12. Comparison of various analytical solutions with the FE creep damage predictions, showing the variations of F/σ_{eq} with the punch displacement. (In this figure, the membrane equivalent stress is evaluated at the contact edge).

$$\Delta = R(1-\cos\theta_0) + Rsin^2\theta_0 \ln\left(\frac{\tan(\theta_0/2)}{\tan(\theta/2)}\right) \tag{47}$$

$$\sigma_{m=} \quad \frac{F}{2\pi RT_0}\frac{\sqrt{1+\frac{1}{(\tan\gamma)^2}}}{\cos\gamma} \tag{48}$$

$$\Delta \ = a_p\left(\frac{1}{\tan\gamma} - \frac{R}{a_p}\left(\frac{1}{\sin\gamma}-1\right)\right) \tag{49}$$

where γ represents half of the cone angle $\left(\frac{\pi}{4} < \gamma < \frac{\pi}{2}\right)$, as demonstrated schematically by Fig. 11. The other symbols are as defined earlier.

Fig. 12 compares our analytical solutions with those proposed by Chakrabarty and by Hyde and Sun *et al.* In this figure, the results obtained from the FE creep damage analysis are taken as a reference/benchmark. As shown, our proposed solution provides a much improved theoretical representation of the small punch creep problem compared with these existing solutions. Further, one can see that although the geometrical relations proposed by Chakrabarty and by Hyde and Sun et al. can provide useful insights into the likely creep behaviour, they are less accurate than the proposed solutions in modelling the small punch creep behaviour. This can be attributed to the fact that the proposed solutions offer a clearer physical meaning by linking the material response to creep damage properties. It may be noted that during the early stage of creep, all the membrane-based solutions (including those derived in the present study) may provide limited prediction capability in view of the anticipated bending effects at the earlier stage of deformation.

5.2. *Applications of the model for creep data correlation*

One of the key merits of the present analytical solution is that it offers opportunities to effectively correlate the small punch creep test data with those obtained via the conventional uniaxial creep tests in an analytical manner using the close form approximations proposed in Section 3.4.3 (i.e., without the need to convert the displacement-time data obtained via SPCT into an equivalent uniaxial strain vs time data), thereby improving the reliability of SPCT data interpretation. For instance, our analytical solution reveals a correlation between the uniaxial creep damage parameters B, χ (which are related to the tertiary creep behaviour), and creep rupture data obtained from SPCTs. That is to say, the parameter χ can be identified from the gradient of log-log plot of the SPCT creep rupture life vs punch load, while B is related to the intercept. Besides, a correlation is present between the secondary stage creep properties (A_1, n_1) obtained from conventional uniaxial creep test and those derived from SPCTs. The creep exponent n_1 can be evaluated from the logarithmic plot of the SPCT minimum displacement rate vs punch loading, while the parameter, A_1, is related to the intercept of the line. It is worth mentioning that the uniaxial creep parameters illustrated above are typically determined on the basis of uniaxial creep tests, which require large volume of materials and enormous test time. Therefore, the suggested analytical approach for data correlation could be an effective mean for creep properties estimation from miniaturized small punch creep tests directly. To further demonstrate the feasibility of our approach, some examples are given as to how our theoretical model can be utilized to determine some key uniaxial creep properties from SPCTs directly. The experimental data stets used here are collected from the literature and

(a)

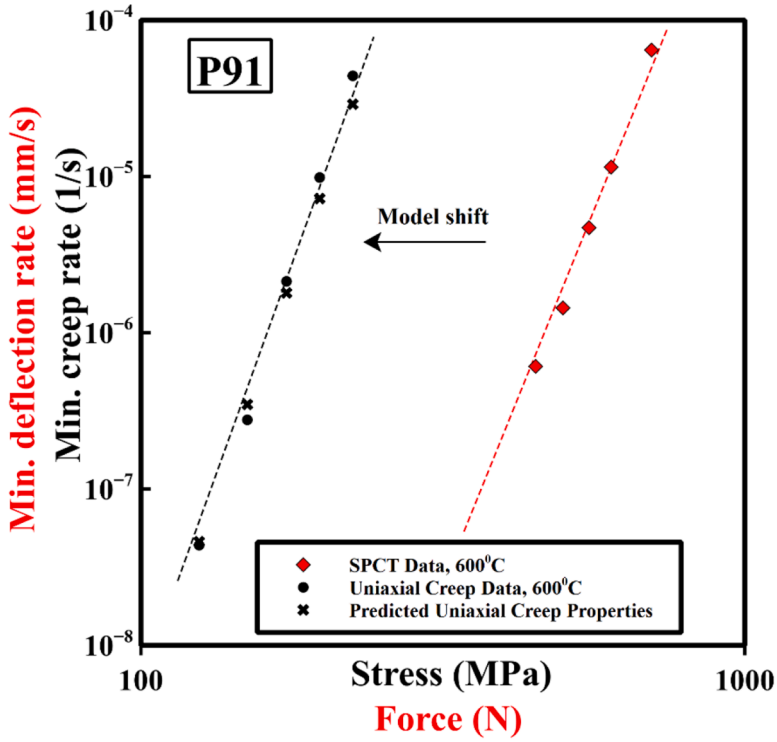

(b)

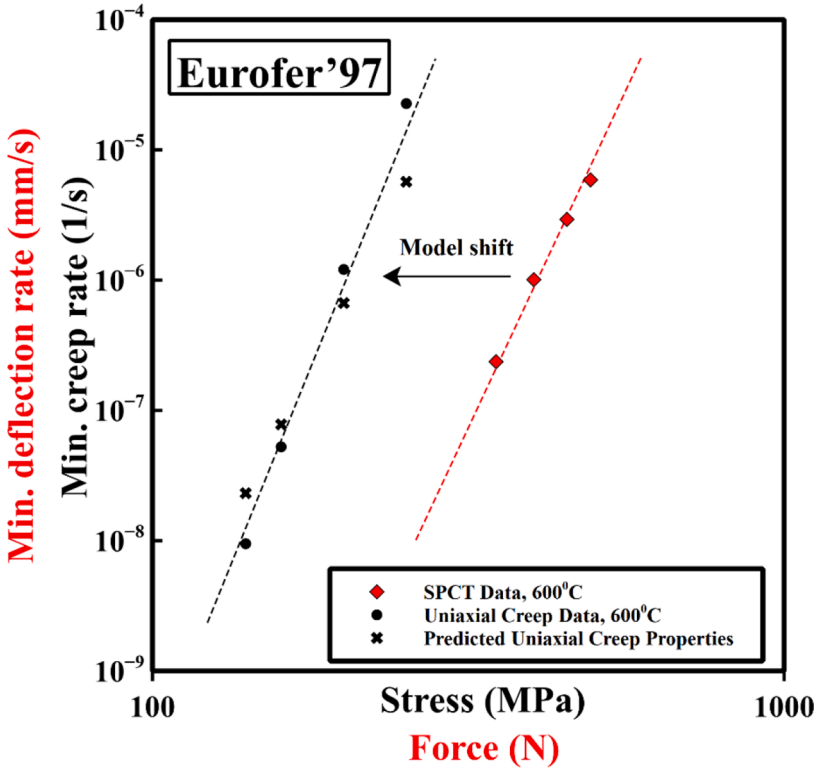

(caption on next page)

Fig. 13. a) Examples illustrating the application of the analytical model for uniaxial creep properties determination from small punch creep data of a) P91 steel at 600°C, and b) Eurofer˙97 alloy at 600°C. (The experimental data for P91 are taken from ref (Dobeš and Milička, 2009), while those relevant to Eurofer97 alloy are taken from ref (Dobeš and Dymáček, 2016)). The arrow in each figure indicates how the small punch creep data are shifted by the model to predict the uniaxial creep behaviour. .

related to two important martensitic steel grades: P91 steel (Dobeš and Milička, 2009) at 600°C and Eurofer97 alloy at 600°C (Dobeš and Dymáček, 2016). The creep behaviours of these materials were characterised separately by means of conventional uniaxial creep tests and small punch creep tests and the relevant testing procedures were published in detail in ref (Dobeš and Milička, 2009) and ref (Dobeš and Dymáček, 2016) for P91 steel and Eurofer97, respectively. Constant force small punch creep tests were performed on the above-named materials at 600°C (Dobeš and Milička, 2009; Dobeš and Dymáček, 2016) using a test setup with the following main dimensions: (Specimen diameter of 8 mm, specimen thickness of 0.5 mm, receiving hole radius of 2 mm, and punch ball radius of 1.25 mm). These tests were complemented by constant load tensile creep tests at 600°C (Dobeš and Milička, 2009; Dobeš and Dymáček, 2016). The relevant data for small punch creep tests for P91 and Eurofer97 are respectively presented in Fig. 13a and Fig. 13b in terms of minimum displacement rate (mm/s) on the y-axis against the applied load (N) on the x-axis (as shown in red). On the other hand, the data obtained from the conventional uniaxial creep tests are plotted in Fig. 13a and Fig. 13b for P91 and Eurofer97, respectively, in terms of the minimum creep rate (1/s) on the y-axis against the applied stress (MPa) on the x-axis, as shown in black. Using the approximate model, given by Eq. (43), the key parameters characterising the uniaxial creep behaviour can be obtained directly by measuring the slope and intercept of the regression line corresponding to small punch creep tests data. To assess the capability of the model in predicting the uniaxial creep behaviour, the model predictions are compared against the experimental data measured from conventional uniaxial creep tests as shown in Fig. 13a and Fig. 13b. It can be seen that the uniaxial creep properties for both P91 steel and Eurofer97 alloy are reasonably predicted by the model.

Lastly, it is worth mentioning that the present theoretical work could also be conveniently used in the experimental design of small punch creep tests. As well known, creep deformation and damage mechanisms exhibit stress dependency. Therefore, choosing an appropriate stress level is crucial for accurate and consistent data correlation (Tu et al., 2019). By utilizing our theory, which describes the relationship between punch loading, stress, strain, creep damage…etc., one can get useful insights into the appropriate test conditions with the desired stress level to obtain more reliable creep properties. In future work, the proposed conversion relationships will be further examined under the effects of friction, initial plasticity, and softening.

5.3. Concluding remarks

Motivated by the lack of a mechanistic based theoretical description of the thin-disk small punch creep problem in the literature, membrane stretching-based creep damage analytical solutions were derived in this study to represent the full stage creep deformation and creep damage which occur over the small punch creep test. The predictive capability of the proposed theory was numerically evaluated using FE creep damage analysis. Here, we only focused on the recommended specimen size by the CEN code of practice (CEN 2006). The proposed solutions represent a first key step towards improved theoretical modelling of the SPCT for ductile materials and enable an improved understanding into the mechanics of the small punch creep. The key conclusions drawn from the present study are:

a) Excellent agreement was obtained between the proposed analytical solutions and the FE creep damage solutions.
b) It was demonstrated that the relationship between the minimum deflection rate and applied loading and the relationship between creep rupture lives and applied loading in small punch creep tests can be analytically described by a power law function, which agree well with experimental data obtained from SPCTs.
c) Compared with other existing analytical solutions in the literature, the proposed solutions have shown to be much more accurate, and can represent full stages creep deformation, with fully defined creep and damage material properties.
d) The theoretical analysis presented in this study suggests that the uniaxial creep properties in principle can be analytically inversed from the SPCTs data, potentially leading to the development of novel and convenient SPCT data interpretation methods.

Yet, there is still room for future development to further consider the complex interactions of the non-linear behaviours which occur over the small punch creep test. Important issues may include the effect of contact friction and the initial plasticity and the inclusion of creep ductility in creep damage constitutive equations. Moreover, to improve the predictive capability of the present solutions, a more generalised model accounting for the size effect is crucial.

CRediT authorship contribution statement

Raheeg Ragab: Conceptualization, Methodology, Software, Formal analysis, Investigation, Data curation, Writing – original draft. **Tao Liu:** Methodology, Writing – review & editing, Supervision, Project administration, Funding acquisition. **Ming Li:** Supervision. **Wei Sun:** Conceptualization, Methodology, Writing – review & editing, Supervision, Project administration, Funding acquisition.

Declaration of Competing Interest

The authors declare that they have no known competing financial interests or personal relationships that could have appeared to influence the work reported in this paper.

Acknowledgments

This work was supported by the Engineering and Physical Sciences Research Council (EPSRC). The funding is provided through the EPSRC Centre for Doctoral Training in Resilient Decarbonised Fuel Energy Systems (Grant number: EP/S022996/1). The work was also partly sponsored by the Net Zero Research.

APPENDIX. Chakrabarty's Membrane Stretching Theory

A Strain solutions in the contact and unsupported regions of the blank (Chakrabarty, 1970)

In Chakrabarty's membrane stretching theory, the circumferential and meridional strains of a given element are generally defined using the logarithmic strain expressions, as given below:

$$\varepsilon_c = \ln\left(\frac{r}{r_0}\right) \tag{A.1}$$

$$\varepsilon_r = \ln\left(\frac{\partial r}{\partial r_0} sec\phi\right) \tag{A.2}$$

where ε_c and ε_r are the circumferential and meridional strains, respectively; r and r_0 denote the current and initial radius, respectively. while the compressive thickness strain, ε_t, is the sum of both the circumferential and meridional strains as defined by the following:

$$\varepsilon_t = \ln\left(\frac{T_0}{T}\right) = \varepsilon_c + \varepsilon_r \tag{A.3}$$

Assuming a balanced biaxial stress state (under friction free contact conditions) and adopting the Levy-Mises flow rule, complete solutions were derived for the circumferential, meridional and compressive thickness strain along the contact region of the blank, i.e., in the range $0 \le \phi \le \theta_0$, as given by Equations (A.4) and (A.5):

$$\varepsilon_c = \varepsilon_r = \ln\left(\frac{(1+\cos\phi)(1+\cos\theta)}{(1+\cos\theta_0)^2}\right) \tag{A.4}$$

$$\varepsilon_t = \ln\left(\frac{T_0}{T}\right) = \varepsilon_c + \varepsilon_r = 2\varepsilon_c \tag{A.5}$$

Similar expressions were derived for the unsupported region, defined by the range $\theta \le \phi \le \theta_0$, as illustrated by Equations (A.6) and (A.7):

$$\varepsilon_c = \varepsilon_r = \ln\left(\frac{1+\cos\theta}{1+\cos\phi}\right) \tag{A.6}$$

$$\varepsilon_t = \ln\left(\frac{T_0}{T}\right) = \varepsilon_c + \varepsilon_r = 2\ln\left(\frac{1+\cos\theta}{1+\cos\phi}\right) \tag{A.7}$$

in which T_0 is the initial blank thickness; T is the current thickness. The other symbols are as defined earlier.

References

Manahan, M.P., 1983. A new post-irradiation mechanical-behavior test-the miniaturized disk bend test. Nucl. Technol. 63 (2), 295–315.
Parker, J.D., James, J.D., 1994. Creep behaviour of miniature disc specimens of low alloy steel, *In Developments in a progressing technology*. PVP 279, 167–172.
Hyde, T.H., Sun, W., Becker, A.A., 1996. Analysis of the impression creep test method using a rectangular indenter for determining the creep properties in welds. Int. J. Mech. Sci. 38, 1089–1102 https://doi.org/10.1016/0020-7403(95)00112-3.
Hyde, T.H., Sun, W., 2009. A novel, high sensitivity, small specimen creep test. The Journal of Strain Analysis for Engineering Design 44 (3), 171–185. https://doi.org/10.1243/03093247JSA502.
Sun, W., Hyde, T.H., 2010. Determination of secondary creep properties using a small ring creep test technique. Metall J LXIII, 185–193.
Morris, A., Cacciapuoti, B., Sun, W., 2018. The role of small specimen creep testing within a life assessment framework for high temperature power plant. Int. Mater. Rev. 63 (2), 102–137. https://doi.org/10.1080/09506608.2017.1332538.
Rouse, J.P., Cortellino, F., Sun, W., et al., 2013. Small punch creep testing: review on modelling and data interpretation. Mater. Sci. Technol. 29 (11), 1328–1345. https://doi.org/10.1179/1743284713Y.0000000278.

Wen, W., Jin, X., Liu, H., Sun, W., 2019a. Determination of creep damage properties from small punch creep tests considering pre-straining effect using an inverse approach. Mech. Mater. 139, 103171 https://doi.org/10.1016/j.mechmat.2019.103171.
Al-Abedy, H., Jones, A., Sun, W., 2018. Small punch creep property evaluation by finite element of Kocks-Mecking-Estrin model for P91 at elevated temperature. Theor. Appl. Fract. Mech. 98, 244–254. https://doi.org/10.1016/j.tafmec.2018.10.006.
Kumar, J.G., Laha, K., 2015. Small Punch Creep deformation and rupture behavior of 316L(N) stainless steel. Materials Science and Engineering: A 641, 315–322. https://doi.org/10.1016/j.msea.2015.06.053.
Chen, H., Al-Abedy, H.K., Li, H., Yang, R., Sun, W., Jones, I.A., 2020. On the deformation and fracture mechanisms of the P91 steel during small punch tensile testing. Mater. Charact. 168, 110514 https://doi.org/10.1016/j.matchar.2020.110514.
Leclerc, N., Khosravani, A., Hashemi, S., Miracle, D.B., Kalidindi, S.R., 2021. Correlation of Measured Load-Displacement Curves in Small Punch Tests with Tensile Stress-Strain Curves. Acta Mater. 204, 116501 https://doi.org/10.1016/j.actamat.2020.116501.
Peng, J., Vijayanand, V.D., Knowles, D., Truman, C., Mostafavi, M., 2021. The sensitivity ranking of ductile material mechanical properties, geometrical factors, friction coefficients and damage parameters for small punch test. Int. J. Press. Vessels Pip. 193, 2021. https://doi.org/10.1016/j.ijpvp.2021.104468.
Pham, H.T., Iwamoto, T., 2018. An evaluation of fracture properties of type-304 austenitic stainless steel at high deformation rate using the small punch test. Int. J. Mech. Sci. 144, 249–261. https://doi.org/10.1016/j.ijmecsci.2018.05.056, 2018.
Lancaster, R.J., Jeffs, S.P., Illsley, H.W., Argyrakis, C., Hurst, R.C., Baxter, G.J., 2019. Development of a novel methodology to study fatigue properties using the small punch test. Materials Science and Engineering: A 748, 21–29. https://doi.org/10.1016/j.msea.2019.01.074.
Gülçimen, B., Hähner, P., 2013. Determination of creep properties of a P91 weldment by small punch testing and a new evaluation approach. Materials Science and Engineering: A 588, 125–131. https://doi.org/10.1016/j.msea.2013.09.029.
Rabenberg, E.M., Jaques, B.J., Sencer, B.H., Garner, F.A., Freyer, P.D., Okita, T., Butt, P., 2014. Mechanical behavior of AISI 304SS determined by miniature test methods after neutron irradiation to 28dpa. J. Nucl. Mater. 448 (1–3), 315–324. https://doi.org/10.1016/j.jnucmat.2014.02.018.
Jackson, G.A., Bai, M., Pala, Z., Hussain, T., Sun, W., 2019a. Small punch creep testing of thermally sprayed Stellite 6 coating: a comparative study of as-received vs. post-heat treatment. Materials Science & Engineering A 747, 137–147. https://doi.org/10.1016/j.msea.2019.02.030.
Wen, W., Jackson, G., Li, H., Sun, W., 2019b. An experimental and numerical study of a CoNiCrAlY coating using miniature specimen testing techniques. Int. J. Mechanical Science 157-158, 348–356. https://doi.org/10.1016/j.ijmecsci.2019.04.001.
Torres, J., Gordon, A.P., 2021. Mechanics of the small punch test: a review and qualification of additive manufacturing materials. J. Mater. Sci. 56, 10707–10744. https://doi.org/10.1007/s10853-021-05929-8.
Hyde, T.H., Hyde, C.J., Sun, W., 2013. Theoretical basis and practical aspects of small specimen creep testing. The Journal of Strain Analysis for Engineering Design 48 (2), 112–125. https://doi.org/10.1177/0309324712463299, 2013.
Calaf-Chica, J., Palomar, M.S., Díez, P.M.B., Calzada, M.P., 2021. Deviations in yield and ultimate tensile strength estimation with the Small Punch Test: numerical analysis of pre-straining and Bauschinger effect influence. Mech. Mater. 153 https://doi.org/10.1016/j.mechmat.2020.103696.
Dymáček, P., Dobeš, F., Jirásková, Y., Pizúrová, N., Friák, M., 2019. Tensile, creep and fracture testing of prospective Fe-Al-based alloys using miniature specimens. Theor. Appl. Fract. Mech. 99 https://doi.org/10.1016/j.tafmec.2018.11.005.
Zhao, L., Song, K., Xu, L., Han, Y., Jing, H., Li, H., Zhang, Y., 2019a. Investigating creep rupture and damage behavior of 41Fe-25.5Cr-23.5Ni alloy small punch creep specimens using a novel microstructure meshing approach. Materials Science and Engineering: A 766. https://doi.org/10.1016/j.msea.2019.138370.
Song, K., Zhao, L., Xu, L., Han, Y., Hongyang Jing, H., 2019. Experimental and numerical analysis of creep and damage behavior of P92 steel by small punch tests. Theor. Appl. Fract. Mech. 100, 181–190. https://doi.org/10.1016/j.tafmec.2019.01.013.
Ortiz-Mariscal, A., Saucedo-Muñoz, M.L.Naveena, Komazaki, S, 2018. Application of small punch creep testing for evaluation of creep properties of as-received and artificially aged 5Cr-0.5Mo steel. Materials Science and Engineering: A 709, 322–329. https://doi.org/10.1016/j.msea.2017.10.060.
Yang, S., Ling, X., Xue, L., 2018. Application of small punch test to investigate mechanical behaviours and deformation characteristics of Incoloy800H. J. Alloys Compd. 765, 497–504. https://doi.org/10.1016/j.jallcom.2018.06.243.
Cortellino, F., Rouse, J.P., Cacciapuoti, B., et al., 2017. Experimental and Numerical Analysis of Initial Plasticity in P91 Steel Small Punch Creep Samples. Exp. Mech. 57, 1193–1212. https://doi.org/10.1007/s11340-017-0296-9.
Cacciapuoti, B., Sun, W., McCartney, D.G., 2016. A study on the evolution of contact angle of small punch creep test for ductile materials. Int. J. Pres. Ves. & Piping 145, 60–74. https://doi.org/10.1016/j.ijpvp.2016.06.002, 2016.
Cortellino, F., Sun, W., Hyde, T., 2016. On the effects of friction modelling on small punch creep test responses: a numerical investigation. The Journal of Strain Analysis for Engineering Design 51 (7), 493–506. https://doi.org/10.1177/0309324716655661.
Ma, Y.W., Shim, S., Yoon, K.B., 2009. Assessment of power law creep constants of Gr91 steel using small punch creep tests. Fatigue & Fracture of Engineering Materials & Structures 32, 951–960. https://doi.org/10.1111/j.1460-2695.2009.01394.x.
Jackson, G.A., Sun, W., McCartney, D.G., 2019b. The influence of microstructure on the ductile to brittle transition and fracture behaviour of HVOF NiCoCrAlY coatings via SP tensile testing. Materials Science & Engineering: A 754, 479–490. https://doi.org/10.1016/j.msea.2019.03.108.
CEN, 2006. CWA 15627 Workshop agreement: Small Punch Test Method For Metallic Materials. European Committee for Standardisation.
Hyde, T.H., Stoyanov, M., Sun, W., Hyde, C.J., 2010a. On the interpretation of results from small punch creep tests. The Journal of Strain Analysis for Engineering Design 45 (3), 141–164. https://doi.org/10.1243/03093247JSA592.
Hyde, T.H., Sun, W., Williams, J.A., 2007. Requirements for and use of miniature test specimens to provide mechanical and creep properties of materials: a review. Int. Mater. Rev. 52 (4), 213–255 https://doi.org/10.1179/174328007 × 160317.
Dyson, C., Sun, W., Hyde, C.J., Brett, S.J., Hyde, T.H., 2016. Use of small specimen creep data in component life management: a review. Mater. Sci. Technol. 32 (15), 1567–1581. https://doi.org/10.1080/02670836.2015.1132536.
Lee, T., Ibupoto, F.A., Lee, J.H., et al., 2016. A Direct Methodology for Small Punch Creep Test. Exp. Mech. 56, 395–405. https://doi.org/10.1007/s11340-015-0108-z, 2016.
Chakrabarty, J., 1970. A theory of stretch forming over hemispherical punch heads. Int. J. Mech. Sci. 12 (4), 315–325 https://doi.org/10.1016/0020-7403(70)90085-8.
Yang, Z., Wang, Z.W., 2003. Relationship between strain and central deflection in small punch creep specimens. Int. J. Press. Vessels Pip. 80 (6), 397–404 https://doi.org/10.1016/S0308-0161(03)00069-3.
Li, Y., Šturm, R., 2006. Small Punch test for weld heat affected zones. Mater. High Temp. 23 (3–4), 225–232. https://doi.org/10.1179/mht.2006.019. DOI:
Yang, S., Ling, X., Zheng, Y., 2017. Creep behaviours evaluation of Incoloy800H by small punch creep test. Mater. Sci. Eng. A 685, 1–6. https://doi.org/10.1016/j.msea.2016.12.092.
Zhao, L., Song, K., Xu, L., Han, Y., Jing, H., Zhang, Y., Li, H., 2019b. Determination of creep properties of an advanced Fe-Cr-Ni alloy using small punch creep test with a modified creep strain model. Theor. Appl. Fract. Mech. 104 https://doi.org/10.1016/j.tafmec.2019.102324.
Liu, Y., Murakami, S., 1998. Damage localisation of conventional creep damage models and proposition of a new creep damage analysis. JSME Int. J. of Solid Mechanics & Material Engineering, Series A 41 (1), 57–65 https://doi.org/10.1299/jsmea.41.57 https://doi.org/10.1299/jsmea.41.57.
Kachanov, L., 1958. On rupture time under condition of creep. *Izvestia Akademi Nauk USSR*, Otd. Techn. Nauk, Moskwa 8, 26–31.
Rabotnov, Y.N. (1969) Creep problems in structural members. Amsterdam: North-Holland; 1969. - 836 p.
Hutchinson, J.W., 1983. Constitutive behavior and crack tip fields for materials undergoing creep-constrained grain boundary cavitation. Acta Metall. 31 (7), 1079–1088.
Riedel, H., 1987. Fracture At High Temperatures. Springer.
Kassner, M.E., Hayes, T.A., 2003. Creep cavitation in metals. Int. J. Plast. 19 (10), 1715–1748 https://doi.org/10.1016/S0749-6419(02)00111-0.
Abstoss, K.G., Schmigalla, S., Schultze, S., Mayr, P., 2019. Microstructural changes during creep and aging of a heat resistant MARBN steel and their effect on the electrochemical behaviour. Materials Science and Engineering: A 743, 233–242. https://doi.org/10.1016/j.msea.2018.11.075.

Ragab, R., Parker, J., Li, M., Liu, T., Morris, A., Sun, W, 2022. Requirements for and challenges in developing improved creep ductility-based constitutive models for tempered martensitic CSEF steels. Journal of Materials Research and Technology 17. https://doi.org/10.1016/j.jmrt.2022.02.047.

Kachanov, L.M., 1986. *Introduction to Continuum Damage mechanics. Mechanics of Elastic Stability*, **Vol 10**. Springer, Dordrecht. https://doi.org/10.1007/978-94-017-1957-5.

Hyde, T.H., Saber, M., Sun, W., 2010b. Testing and modelling of creep crack growth in compact tension specimens from a P91 weld at 650 °C. Eng. Fract. Mech. 77 (15), 2946–2957. https://doi.org/10.1016/j.engfracmech.2010.03.043.

Ragab, R., Parker, J., Li, M., Liu, T., Sun, W., 2021. Modelling of a Grade 91 Power Plant Pressurised Header Weldment under Ultra Super-Critical Creep Conditions. Int. J. Press. Vessels Pip. 192, 104389 https://doi.org/10.1016/j.ijpvp.2021.104389.

Zhai, P., Hashida, T., Komazaki, S., Zhang, Q., 2004. Numerical Analysis for Small Punch Creep Tests by Finite-Element Method. J. Test. Eval. 32 (4), 298–303. https://doi.org/10.1520/JTE12250.

ABAQUS 2019 online documentation. (2019) © Dassault Systèmes.

Dobeš, F., Milička, K., 2009. Application of creep small punch testing in assessment of creep lifetime. Mater. Sci. Eng. A 510–511, 440–443. https://doi.org/10.1016/j.msea.2008.04.087.

Dobeš, F., Dymáček, P., 2016. Fracture-based correlation of uniaxial and small punch creep data. Theor. Appl. Fract. Mech. 86, 34–38. https://doi.org/10.1016/j.tafmec.2016.08.020.

Tu, S.-.T., Zhang, K., Bai, Y., Tan, J.-.P., Deng, G.-.J., 2019. Effect of stress regime-dependent creep behaviour on measurement of creep strain rate based on small specimen techniques. Fatigue Fract. Eng. Mater. Struct. 42 (187–196) https://doi.org/10.1111/ffe.12894.